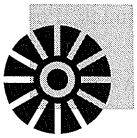

Contributed Paper

Characteristics of a Supersonic Plasma Flow in a Magnetic Nozzle

INUTAKE Masaaki, ANDO Akira, HATTORI Kunihiko, TOBARI Hiroyuki and YAGAI Tsuyoshi
Department of Electrical Engineering, Tohoku University, Sendai, 980-8579, Japan

(Received 30 May 2002 / Accepted 21 October 2002)

Abstract

A high-density and high-speed flowing helium-plasma is produced quasi-steadily (1 ms) by use of a magneto-plasma-dynamic arcjet (MPDA) in various external magnetic field configurations. In a uniform magnetic field configuration, an ion acoustic Mach number M_i of the plasma flow is limited to be nearly unity. In a divergent magnetic nozzle configuration, on the other hand, the Mach number increases up to almost 3. The Mach number increases in proportion to the gradient of the magnetic field. Spatial variations of M_i are well predicted by an isentropic model of compressible flow. The Mach number decreases in the downstream region due to charge-exchange collisional processes that are caused by a limited pumping capability of surface-recombined neutral gases.

Keywords:

MPD arcjet, magnetic nozzle, plasma acceleration, Mach number, Mach probe, HITOP, supersonic plasma flow, isentropic model

1. Introduction

Dramatic Magneto-Hydro-Dynamic (MHD) phenomena in space and fusion plasmas have been observed as the result of recent developments in plasma diagnostics. Violent activities near the solar surface have stimulated much interest in this field, especially in magnetic reconnection, plasma acceleration, and shock wave phenomena [1,2]. High-speed flow effect on equilibrium in a fusion plasma is also a current topic of interest [3]. Production and study of a high-beta, supersonic plasma flow with a magnetic field is quite important for basic research on MHD phenomena in space and fusion plasmas.

Recently, an electric propulsion system was developed for various space missions. The magneto-plasma-dynamic arcjet (MPDA) is a promising electric propulsion device that has relatively large thrust and high specific impulse [4].

One method by which to increase the performance of an MPDA is to operate it in an externally applied magnetic field [5-8]. A plasma in a divergent magnetic nozzle is expected to be accelerated by converting thermal energy to flow energy.

There are several acceleration mechanisms for an MPDA with an externally applied magnetic field [4]. A plasma in the MPDA is accelerated axially by $J_r \times B_\theta$ force, where J_r is a radial discharge current and B_θ is a self-induced azimuthal magnetic field. In a magnetic field B_z applied externally in the axial direction, the interaction between B_z and J_r results in an azimuthal electromagnetic force $J_r \times B_z$, which drives the plasma to rotate azimuthally. The swirling flow energy can be converted into axially flowing energy through a magnetic nozzle formed by the applied magnetic field.

author's e-mail: inutake@ecei.tohoku.ac.jp

この論文は第18回年会(2001, 福岡県春日市)にて招待講演として発表された内容を論文化したものです。

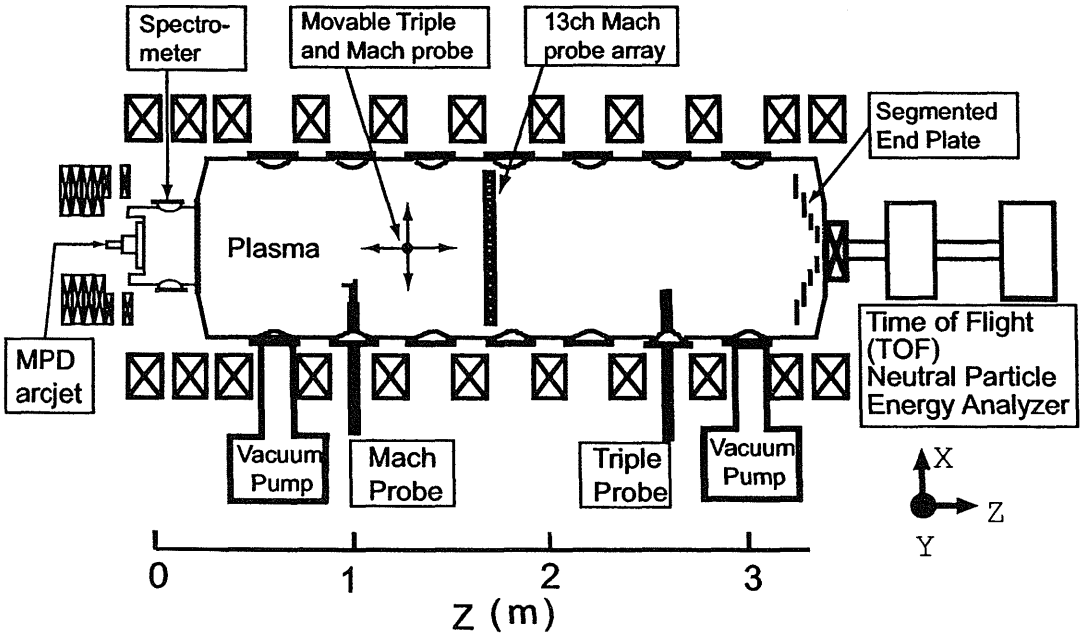

Fig. 1 Schematic view of the HITOP device.

Moreover, under appropriate conditions, azimuthally-induced electron Hall current J_θ interacts with B_r to accelerate the plasma in the axial direction [9].

It is very important to investigate a plasma flow field in a magnetic nozzle not only to clarify various acceleration mechanisms of the MPDA but also to realize a quasi-steady supersonic plasma flow for basic plasma physics experiments on MHD phenomena.

We herein report the characteristics of a plasma flow produced by an MPDA in various magnetic nozzle configurations. Spatial variations of an ion Mach number M_i are discussed in terms of both the particle model and the isentropic fluid model. The effect of collisional processes caused by neutral gas is also estimated.

2. Experimental Apparatus

A high power, quasi-steady MPDA device was installed in the HITOP (HIgh density TOhoku Plasma) device of Tohoku University, as shown in Fig. 1. The HITOP device consists of a large cylindrical vacuum chamber (diameter D = 0.8 m, length L = 3.3 m) with eleven main and six auxiliary magnetic coils, which can generate a uniform magnetic field up to 0.1 T. Various types of magnetic field configurations can be formed by adjusting the external coil current [10].

The MPDA, which is installed at one end port of the HITOP device, has a coaxial structure with a center tungsten rod cathode (10 mm diam.) and an annular molybdenum anode (30 mm diam.), as shown in Fig. 2. A fast-acting gas valve can inject helium gas quasi-steadily for 3 ms with a rise and fall time of 0.2 ms. Time evolution of the gas pressure near the muzzle of the MPDA is measured by use of a semiconductor pressure sensor in a specially-arranged chamber. Arc discharge between the coaxial electrodes is initiated at 1.4 ms after the gas valve triggering when the gas flow rate becomes quasi-steady. Discharge current I_d up to 10 kA is supplied by a pulse-forming network (PFN)

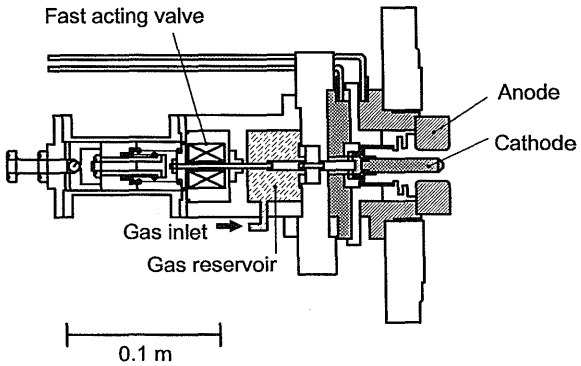

Fig. 2 Schematic view of the MPD arcjet.

system with a quasi-steady duration of 1 ms. The current can be increased to 15 kA with a shorter duration of 0.4 ms. The current I_d is kept nearly constant during the discharge by using a series resister of 100 mΩ, which is much larger than the arc impedance (around 20 mΩ). Thus, I_d can be controlled by varying the charging voltage of the capacitor banks of the PFN power supply. The coordinate direction of the X, Y, and Z axes are shown in Fig. 1. The position $Z = 0$ is located at the tip of the cathode rod of the MPDA, which is located 0.5 cm in from the end surface of the anode.

The plasma is accelerated in the axial (Z-axis) direction by the $\boldsymbol{J} \times \boldsymbol{B}$ force, and expands in the large vacuum chamber. Then a high-density, highly-ionized plasma flow is produced in the HITOP.

Plasma flow characteristics are measured by several diagnostics installed in the HITOP device. Electron temperature and density profiles are measured by a movable triple probe and a fast-voltage-scanning Langmuir probe. A plasma flow is characterized by an ion Mach number M_i, which is defined as the ratio of the plasma flow velocity to the ion acoustic velocity. Profiles of M_i and plasma density along and across the field lines are measured by a movable Mach probe and an array of 13-channel Mach probes set 1.7 m downstream of the MPDA muzzle.

A schematic view of the Mach probe used in this experiment is shown in Fig. 3. The Mach probe has two plane tips, one of which, called the parallel tip, faces the plasma flow direction, and the other, called the perpendicular tip, faces the perpendicular direction [10,11]. The ion Mach number can be directly derived from the ratio of the two ion saturation current densities J_{para} and J_{perp}, which are collected at the parallel and perpendicular tips, respectively, as follows:

$$M_i = \frac{U_z}{C_s} = \frac{U_z}{\sqrt{(\gamma_e T_e + \gamma_i T_i)/m_i}} \quad (1)$$

$$= \kappa \frac{I_{para}}{I_{perp}}. \quad (2)$$

Here, U_z is the plasma flow velocity, C_s is the ion acoustic velocity, m_i is an ion mass, and γ_e and γ_i are the specific heat ratios of electrons and ions, respectively. T_e and T_i are electron and ion temperature, respectively. The coefficient κ should depend on the ratio T_e/T_i and $\kappa = 0.4$ in the case of $T_e = T_i$.

Each tip of the Mach probes is biased –40 V against a conducting wire with a large collection area that is wound around the probe support. The Mach probe is a kind of asymmetric double probe, and an ion saturation current can be measured in spite of the large change in the plasma potential usually observed in the initial phase of the discharge. The effect of the magnetic field was negligible in the ion saturation current in the present experiments, because the ion Larmour radius was much larger than the size of the probe tip.

A spectroscopic technique was used to measure ion temperature T_i and flow velocity U_z near the muzzle of the MPDA. Emission from the plasma was collected by a quartz lens then transferred to a spectrometer by a single fiber cable. The spectrum was detected with an image intensifier tube coupled with a CCD camera (ICCD), which was set at the exit plane of a 1 m Czerny-Turner spectrometer with a grating having 2,400 grooves/mm. HeII line spectra (λ = 468.58 nm) were obtained at 0.1 msec intervals during a shot with a spectral resolution of 0.02 nm. T_i and U_z were obtained from the Doppler broadening and spectral shift of the HeII line [12].

Several other diagnostics were installed in the HITOP device, as shown in Fig. 1. A time-of-flight (TOF) neutral particle energy analyzer was provided at the end of the HITOP along the Z-axis; that is, in the plasma flow direction. Ion temperature and flow velocity of plasmas were also deduced from the TOF data. An array of multi-channel magnetic probes was utilized to measure the magnetic field fluctuations associated with MHD activities in the supersonic plasma.

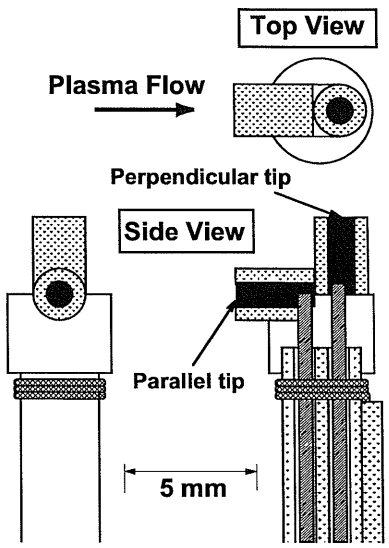

Fig. 3 Schematic view of the Mach probe.

3. Experimental Results

Time evolutions of the HITOP plasma parameters are shown in Fig. 4. The discharge voltage V_d and current I_d are kept nearly constant for 1 ms. Ion saturation current densities, which are measured by a Mach probe located 1.7 m downstream of the MPDA muzzle, J_{para} and J_{perp}, and their ratio are also shown in the figure.

The discharge voltage in the MPDA increases with an increase in the current, as shown in Fig. 5. This is quite different from the conventional thermal-arc characteristic of the voltage decreasing with an increase in the current.

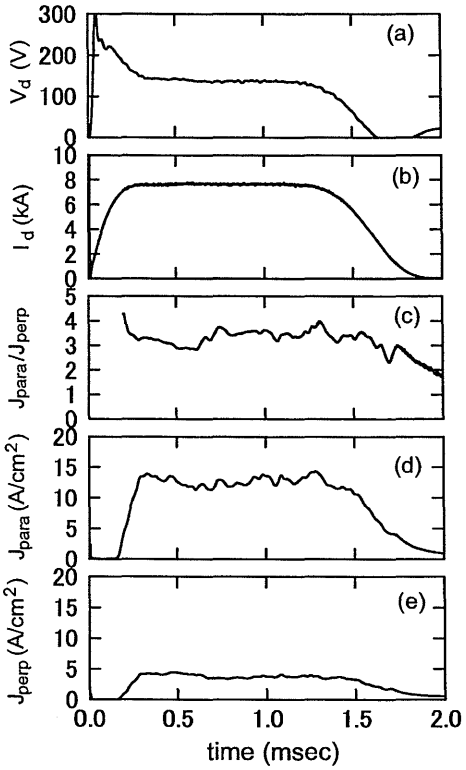

Fig. 4 Time evolutions of the HITOP plasma.

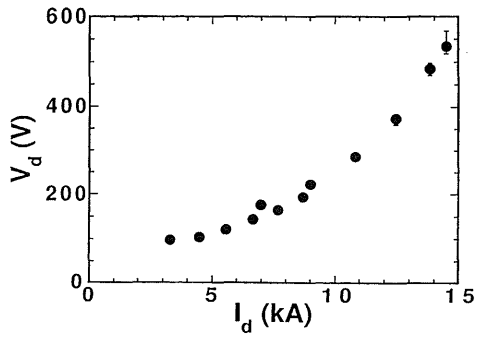

Fig. 5 Dependence of V_d on I_d. B_z = 0.1 T. $\dot{m}$ = 0.12 g/sec.

3.1 Uniform magnetic field configuration

Figure 6 shows time evolutions of I_d, U_z and T_i which are measured near the MPDA by the spectroscopy in the uniform magnetic field configuration. T_i and U_z are almost constant during a shot, and are around 10 eV and 25 km/sec, respectively, when I_d is 8 kA.

The ion Mach number is defined and calculated from the spectroscopically-measured T_i and U_z, as follows:

$$M_i = \frac{U_z}{\sqrt{(\gamma_e T_e + \gamma_i T_i)/m_i}} = \sqrt{\frac{\frac{1}{2}m_i U_z^2}{T_i}} = \sqrt{\frac{W_z}{T_i}}, \quad (3)$$

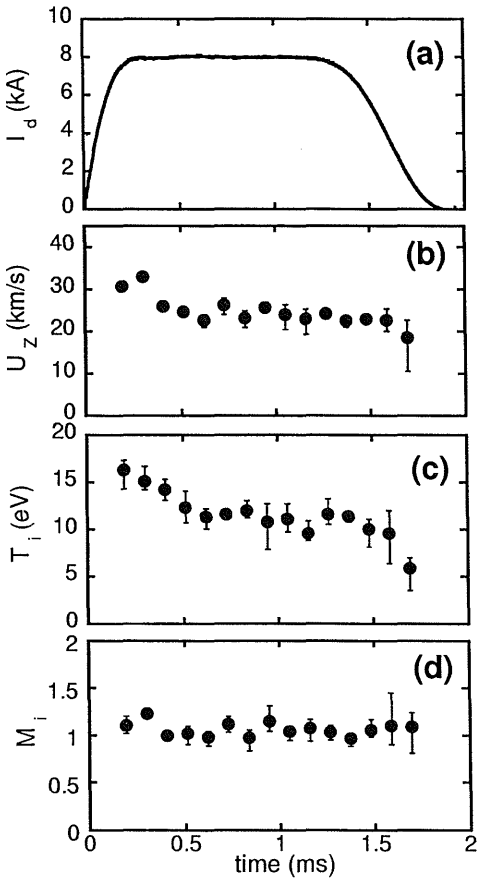

Fig. 6 Time evolutions of (a) I_d, (b) U_z, (c) T_i and (d) M_i spectroscopically measured in a uiform magnetic field configuration. I_d = 8.0 kA, B_z = 0.1 T and $\dot{m}$ = 0.2 g/sec.

where W_z is the flow energy, and $T_e = T_i$ and $\gamma_e = \gamma_i = 1$ are assumed. As shown in Fig. 6(d), the obtained Mach number is almost constant at around $M_i = 1$ in the uniform magnetic field configuration. This result is the same as that measured by Mach probes in the far downstream region. Figure 7 shows dependences of U_{total}, T_i and M_{total} on the current I_d. Here, U_{total} is the total flow velocity calculated as $U_{total} = \sqrt{U_z^2+U_\theta^2}$, where U_θ is the azimuthal flow velocity. As I_d increases, M_{total} increases slightly in a low current ($I_d \leq 5$ kA) region and tends to saturate around $M_{total} = 1$ in a high current region. This indicates that the plasma flow is choked in a uniform magnetic channel.

Electron density n_e and temperature T_e on the flow axis are measured by a fast-voltage-scanning probe and are obtained around $10^{12} \sim 10^{14}$ cm^{-3} and 5 ~ 10 eV, depending on the operating conditions. The electron density increases almost linearly with the increase in I_d and B_z for a certain range of gas flow rate.

3.2 Magnetic nozzle configuration

As mentioned in the introduction, U_z is expected to increase in conjunction with a nozzle configuration of the axial magnetic field. Figure 8(a) shows three types of magnetic nozzle configurations, which have a similar nozzle shape and different nozzle positions. J_{para}/J_{perp} and J_{perp} are shown in Fig. 8(b),(c), respectively. Ion

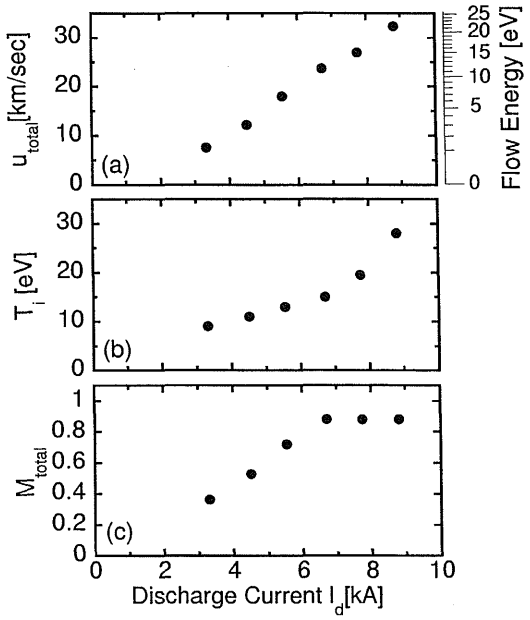

Fig. 7 Dependencies of (a) U_{total} and the flow energy, (b) T_i and (c) M_{total} on I_d in a uniform magnetic field configuration. $B_z = 0.1$ T. $\dot{m} = 0.07$ g/sec.

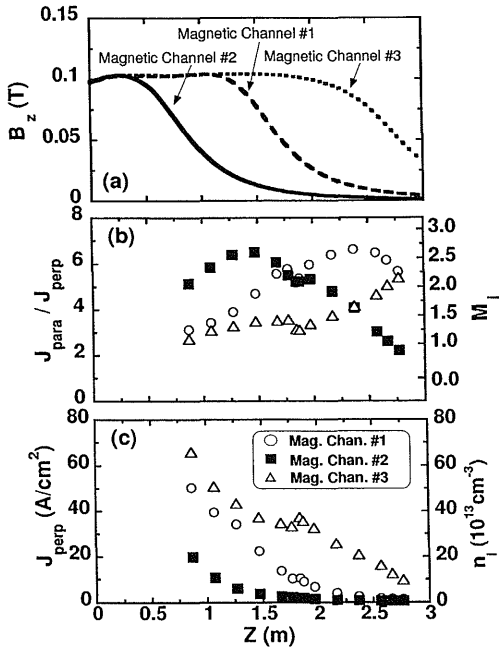

Fig. 8 Axial profiles of (a) three types of nozzle magnetic configurations, (b) J_{para}/J_{perp}, and (c) J_{perp}. Open circles, closed rectangles and open triangles correspond to magnetic channel #1, #2 and #3, respectively. $I_d = 8.8$ kA. $\dot{m} = 0.27$ g/sec.

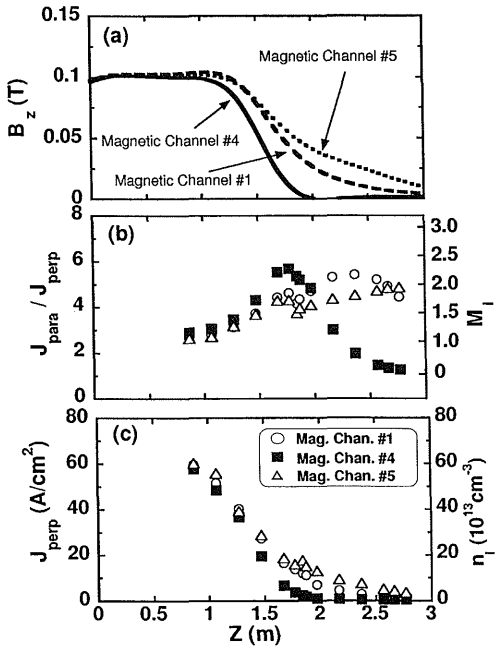

Fig. 9 Axial profiles of (a) three types of nozzle magnetic configurations, (b) J_{para}/J_{perp}, and (c) J_{perp}. Open circles, closed rectangles and open triangles correspond to magnetic channel #1, #4 and #5, respectively. $I_d = 8.8$ kA. $\dot{m} = 0.27$ g/sec.

density n_i, calculated assuming T_e = 5 eV, is also shown in Fig. 8(c). As shown in the figure, the Mach number M_i calculated from J_{para}/J_{perp} increases in the nozzle region. As B_z decreases, M_i increases, reaching almost 3, then decreases to unity. The reason why M_i decreases in the downstream region will be discussed later.

Variations of M_i with the three types of the nozzle configurations with different magnetic field gradients were also measured, as shown in Fig. 9. As the gradient increases, M_i increases more rapidly.

We measured the axial profiles of the U_z and T_i by use of the spectrometer and the TOF analyzer in the magnetic nozzle configuration (magnetic channel #4). Results are shown in Fig. 10(c) and (d). The ion flow velocity and its temperature obtained by the TOF analyzer are also plotted in the figure. Though the TOF signal is the value integrated along the sight-of-view, the location of the main contribution to the signal is estimated at Z = 1.5 m, considering the charge exchange probability and the neutral particle density profile. The flow energy increases by almost 10 eV, which corresponds reasonably to the decrease in T_i.

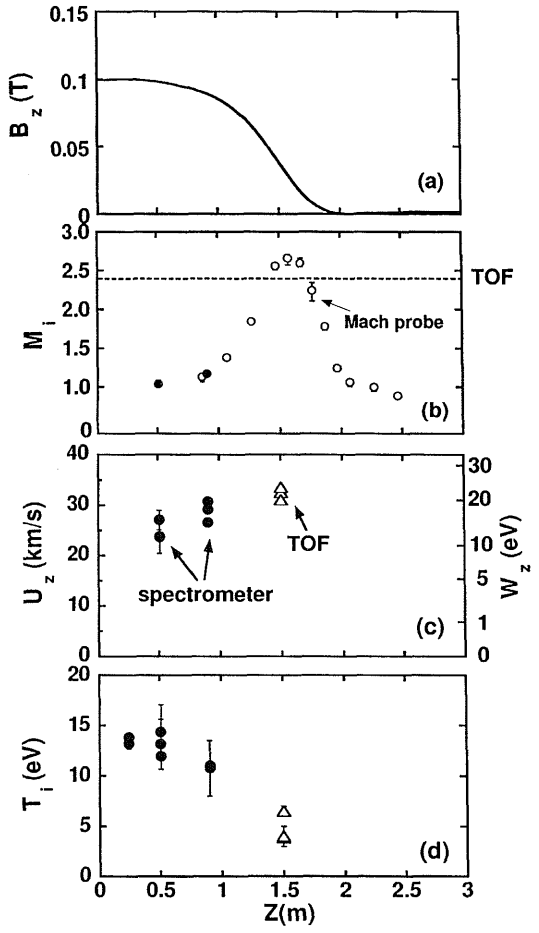

Fig. 10 Axial profiles of (a) the magnetic nozzle configuration #4, (b) M_i, (c) U_z and (d) T_i. Open circles, closed circles and open triangles are the data measured by the Mach probe, the spectrometer and the TOF analyzer, respectively. I_d = 7.0 kA. $\dot{m}$ = 0.13 g/sec.

Mach numbers measured by the Mach probe are plotted by open circles and that calculated from the TOF data is indicated by a dotted line in Fig. 10(b). The Mach number in the upstream region (Z < 90 cm) is also calculated from spectroscopically-obtained U_z and T_i by eq.(3) and plotted by closed circles in the figure. It is noted that the Mach numbers obtained by these three diagnostics are in good agreement with each other.

4. Discussions

Spatial variation of the Mach number is discussed in terms of both the single particle model and the isentropic flow model.

The equation of motion of a singly-charged particle in an axially-magnetized plasma is expressed as follows:

$$m\frac{dv_{||}}{dt} = F_{||} = -\mu\frac{dB_z}{dz}. \quad (4)$$

Here, m is the particle mass and μ is the adiabatic invariant. $F_{||}$ is an axial force driving a particle in the axial direction.

This equation is derived from the conservation law of a kinetic energy $W = \frac{1}{2}mv^2 = \frac{1}{2}m(v_{||}^2 + v_{\perp}^2) = W_{||} + W_{\perp}$ and the adiabatic invariant $\mu = \frac{1}{2}mv_{\perp}^2/B_z = W_{\perp}/B_z$ in the slowly-varying magnetic field. Here, $W_{||} = \frac{1}{2}mv_{||}^2$ is the parallel (axial) energy of an ion and $W_{\perp} = \frac{1}{2}mv_{\perp}^2$ is the perpendicular energy. $W_{\perp}$ is equal to T_i, assuming that ions are thermalized in the perpendicular direction. Ions passing through the magnetic nozzle convert their perpendicular kinetic energy $W_{\perp}$ into axial energy $W_{||}$ to keep W and μ constant. On the other hand, electrons with a faster thermal velocity and a higher collision frequency are considered to be iso-thermal along the field line.

From these conservation laws and the expression of M_i in eq.(3), the following equation is derived:

$$B_z(M_i^2 + 1) = \text{const}. \quad (5)$$

Then M_i at $B_z = B$ is calculated by M_{i0} at $B_z = B_0$ and a mirror expansion ratio $R = B_0/B$, as

$$M_i = \sqrt{(M_{i0}^2 + 1)R - 1}\,. \quad (6)$$

When $M_{i0} = 1$,

$$R = \frac{M_i^2 + 1}{2} . \qquad (7)$$

In a one-dimensional isentropic flow model, on the other hand, the Mach number M_i is related to the variation of the cross section S of the flow, as follows:

$$\frac{dM_i}{M_i} = \frac{2 + (\gamma_i - 1) M_i^2}{2(M_i^2 - 1)} \frac{dS}{S} . \qquad (8)$$

By integrating the eq.(8), the relation of M_i and S can be derived as follows:
for $\gamma_i = 1$,

$$M_i S \exp\left(-\frac{M_i^2}{2}\right) = \text{const} \quad , \quad \text{and} \qquad (9)$$

for $\gamma_i \neq 1$,

$$M_i S \left(1 + \frac{\gamma_i - 1}{2} M_i^2\right)^{-\frac{\gamma_i + 1}{2(\gamma_i - 1)}} = \text{const} . \qquad (10)$$

From the magnetic flux conservation, ($B_z S$ = const), the variation of S is related to the variation of B_z, as

$$\frac{dS}{S} = -\frac{dB_z}{B_z} . \qquad (11)$$

When $M_{i0} = 1$, the mirror ratio R is calculated by M_i from the above equations (9), (10), and (11), and is expressed as follows:
for $\gamma_i = 1$,

$$R = \frac{1}{M_i} \exp\left[\frac{(M_i^2 - 1)}{2}\right] , \quad \text{and} \qquad (12)$$

for $\gamma_i \neq 1$,

$$R = \frac{1}{M_i}\left[\frac{2}{\gamma_i + 1}\left(1 + \frac{\gamma_i - 1}{2} M_i^2\right)\right]^{\frac{\gamma_i + 1}{2(\gamma_i - 1)}} . \qquad (13)$$

In order to compare these two models with experimental data, an axial profile of M_i is measured in the divergent magnetic nozzle configuration shown in Fig. 11(a). Ratios of a plasma radius R_p to an ion Larmour radius ρ_i are calculated and shown in Fig. 11(b). Here, ρ_i is calculated by assuming T_i = 5 eV, and R_p is derived by using the profile data at Z = 1.7 m

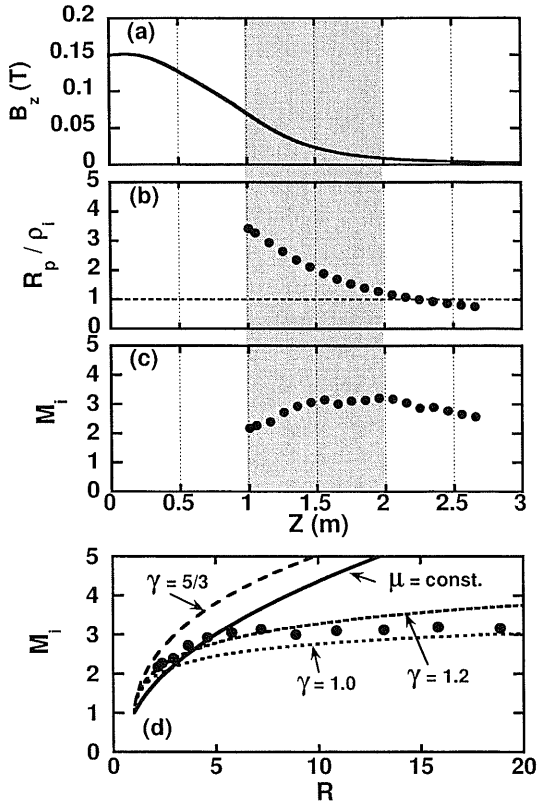

Fig. 11 (a) Axial profiles of the magnetic nozzle configuration, (b) a ratio of the plasma radius R_p to the ion Larmour radius ρ_i and (c) M_i measured at t = 0.3 ms by a movable Mach probe. (d) M_i is plotted as a function of the mirror expansion ratio R. The dashed and solid lines represent the predictions in terms of isentropic flow model and single particle model, respectively. M_i = 1 at Z = 0 and γ_i = 5/3, 1.2, 1.0 are assumed in the calculation. I_d = 8.2 kA. $\dot{m}$ = 0.17 g/sec.

measured by the Mach probe array and the relation of $B_z R_p^2$ = const.

The axial profile of M_i is plotted in Fig. 11(c). The M_i is also plotted as a function of the mirror expansion ratio R(= B_0/B) in Fig. 11(d) by using the data in the hatchmarked region in the figure, where the condition $R_p/\rho_i > 1$ is satisfied. The solid line represents the single particle model (eq.(7)), and the dashed and dotted lines represent the isentropic flow model (eq.(13)) in which M_i = 1 at Z = 0 and γ_i = 5/3, 1.2 and 1.0 are assumed in the calculation, respectively.

These data show that the isentropic flow model predicts well the spatial variation of the Mach number of a plasma flow in the divergent magnetic nozzle. The mean free path of a fast flowing ion to a thermal ion,

λ_{fi-i}, is several cm, and the Hall parameter of an ion, $\omega_{ci}\tau_{fi-i}$, is 1 in this experiment. Because the ions cannot behave as a single particle, the assumption of μ = const is violated. The Hall parameter of an electron, $\omega_{ce}\tau_{ei}$, is several tens in the hatchmarked region. Since the electrons are well magnetized, the cross section of the plasma maintains the relation of B_zS = const and the ions behave as a compressible flow in the divergent nozzle.

Though the specific heat ratio γ is an important parameter in gas dynamics and even in plasmas, there are few publications on γ in plasmas so far. This variable should depend on the number of degrees of freedom f, such that $\gamma = (f + 2)/f$. The value of γ in a plasma is expected to be lower due to an extra degree of freedom caused by the ionization and excitation processes. Burm *et al.* calculated γ in a cascaded arc discharge and showed that γ is nearly 1.2 within a range of ionization degrees of 0.1 to 0.9 [13]. The estimated value of γ in the present experiment agrees well with the calculated one. This coincidence is due to the fact that the ionization degree is expected to be about 0.9 in the present experiments with a higher I_d.

In an axial magnetic field, an MPDA plasma rotates azimuthally by $J_r \times B_z$ force. The swirling flow energy of the plasma is expected to be converted to axial flow energy in the applied divergent nozzle field, and to contribute to the increase in M_i. A radial profile of the plasma rotation speed was measured at 25 cm downstream of the MPDA muzzle by use of the spectrometer. Maximum rotation speed was 10 km/sec, which corresponds to the rotational energy of 2 eV. Therefore, the contribution of the plasma rotation to the increase in M_i is negligibly small under the present experimental conditions.

In the downstream region of the magnetic nozzle, M_i begins to decrease. This phenomenon can be explained based on collisional processes with neutral particles.

As is shown in Figs. 8, 9, and 10, M_i decreases in the region downstream of the magnetic nozzle. These data are taken at t = 1 ms after the discharge trigger. Figure 12 shows time evolutions of the axial profile of M_i. In the earlier phase of the plasma duration, the decrease in M_i cannot be seen. At t = 1 ms, the decrease in M_i appears as shown in the figure. This temporal behavior indicates that neutral particles, generated through the recombination process on the surface of end-plates placed at the end of the HITOP device, diffuse back into the plasma and charge-exchange with

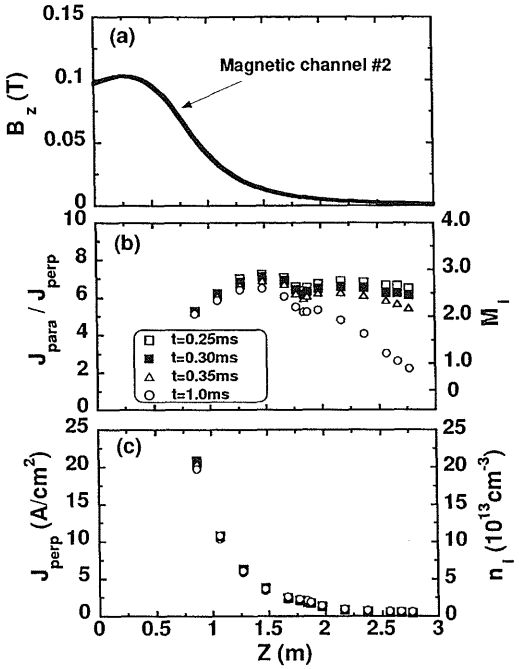

Fig. 12 Temporal evolutions of the axial profiles of (a) the magnetic nozzle configuration #2, (b) J_{para}/J_{perp}, and (c) J_{perp}. I_d = 8.8 kA. $\dot{m}$ = 0.27 g/sec.

fast ions.

As shown in Fig. 12, M_i begins to decrease at Z = 1.5 m. At this point, the plasma radius R_p, calculated under the assumption that $B_zR_p^2$ is constant, is equal to the ionization mean free path of helium neutral atoms (λ_{ae}), which was 10 cm under the present conditions. In the region where the ratio R_p/λ_{ae} is smaller than 1, neutral particles can penetrate into the plasma core region from the peripheral region and charge-exchange with fast ions. It should be noted that neutral particles generated at the end cannot penetrate far into the upstream plasma along the flow axis due to the short-ionization mean free path. This charge-exchange collisional process is also valid in explaining why the velocity measured by TOF is nearly equal to the peak velocity in the expanded region of the magnetic nozzle shown in Fig. 10.

The charge exchange collisions between the fast ions and atoms produce slow ions, decelerate the plasma flow and result in the decrease of M_i. Since the neutral particles generated on the end-plate surface (Z = 3.0 m) move with a thermal velocity determined by the wall temperature, it takes about 1 ms for the particles to diffuse back in the peripheral vacuum region of the

magnetic nozzle (Z = 1.5 m). This explains why there is a time delay of the Mach-number-decreasing phenomena in the region downstream of the magnetic nozzle. To avoid this neutral gas effect in the discussion of the flow model, the data taken at t = 0.3 ms are used in Fig. 11. There are several ways to suppress the charge-exchange effects: first, the length of the vacuum chamber should be sufficiently long; second, the experimental data should be measured in the earlier phase of the discharge; and third, the plasma density in the divergent region of the magnetic nozzle should be sufficiently high for neutrals not to penetrate into the plasma core.

5. Summary

A high density and supersonic plasma flow is produced quasi-steadily by use of a high power (2 MW) MPDA in the HITOP device. We measured several parameters such as the axial and rotational flow velocities and ion/electron temperatures of a plasma from an MPDA in various magnetic configurations.

In a uniform magnetic field configuration, both the ion temperature T_i and the flow velocity U_z increase with an increase of the discharge current I_d. The plasma flow is choked at the Mach number of unity, though I_d increases. The Mach numbers obtained by a Mach probe, a spectrometer, and a time-of-flight energy analyzer agreed well.

The Mach number increases in a magnetic nozzle configuration. An increasing rate of M_i is proportional to the gradient of magnetic field strength, and almost reaches 3. The spatial variation of M_i is expressed in an isentropic flow model in which the plasma flows in the slowly-expanding nozzle. In the later phase of the discharge, M_i decreases in the downstream region due to charge-exchange collisional processes between fast ions and neutral particles, which are generated on the end-plate through a surface recombination process. This is caused by the limited pumping capability of the neutral gas or the limited length of the vacuum chamber.

Acknowledgments

This work was supported in part by a Grant-in-Aid for Scientific Research from the Japan Society for the Promotion of Science. A portion of this work was carried out under the Cooperative Research Project Program of the Research Institute of Electrical Communication, Tohoku University, and the National Institute for Fusion Science. We gratefully acknowledge Drs. T. Shoji and M. Ichimura for their generous cooperation arranging the time-of-flight neutral-particle energy analyzer.

References

[1] R.M. Kulsrud, Phys. Plasmas **2**, 1735 (1995).
[2] E.R. Priest, Phys. Plasmas **4**, 1945 (1997).
[3] S.M. Mahajan and Z. Yoshida, Phys. Rev. Lett. **81**, 4863 (1998).
[4] R.G. Jahn, *Physics of Electric Propulsion* (McGRAW-HILL, 1968).
[5] K. Kuriki and M. Inutake, Phys. Fluids **17**, 92 (1974).
[6] H. Tahara, Y. Kagaya and T. Yoshikawa, J. Propulsion Power **13**, 651 (1997).
[7] K.F. Schoenberg *et al.*, Phys. Plasmas **5**, 2090 (1998).
[8] J.T. Scheuer *et al.*, IEEE Trans. Plasma Phys. **22**, 1015 (1994).
[9] M. Sasoh and Y. Arakawa, J. Propulsion Power **11**, 351 (1995).
[10] M. Inutake *et al.*, *Proc. 10th Int. Congress on Plasma Physics and 42nd APS Meeting*, (Quebec, 2000), ICPP-2000, Vol.**1**, p.148.
[11] A. Ando *et al.*, *Proc. of 25th Int. Conf. on Phenomena in Ionized Gases*, (2001, Nagoya) Vol.**2**, p.195.
[12] A. Ando *et al.*, J. Plasma Fusion Res. SERIES, Vol.**4**, 373 (2001).
[13] K.T.A.L. Burm *et al.*, Phys. Plasmas **6**, 2622 (1999).